Technical Note of Theoretical Study (TN-TS)

SK2-09: Follow-up of feasibility study to observe ionospheric disturbances by airglow monitoring network (AMON-net)

Department of Space Physics
Institute of Experimental Physics, Slovak Academy of Sciences
Košice, Slovakia

ESA Contract No. 4000125330/18/NL/SC,
Plan for European Cooperating States (PECS) in Slovakia
July 2019

Contents

Revision History

Revision	Date	Author(s)	Description
1.0	07. 07. 2019	S. Mackovjak	Submitted version for CDR

Chapter 1

Introduction

1.1 Purpose

The Technical Note of Theoretical Study (TN-TS) is a continuation of theoretical studies performed within the previous activity - "Feasibility study to observe ionospheric disturbances by one pixel UV detector" (SK1-05). It provides a theoretical and scientific background for the R&D activity "Follow-up of feasibility study to observe ionospheric disturbances by airglow monitoring network (AMON-net)" (SK2-09).

1.2 Document Overview

The TN-TS document consists of six major chapters. Basic information about this technical note is in Chapter 1. The summary of the main outcomes from the previous activity - SK1-05 are recapitulated in Chapter 2. The theoretical background for AMON-net is presented in Chapter 3. The overview of historical airglow data that are similar as AMON-net data is provided in Chapter 4. The study of local geomagnetic field dynamics is in Chapter 5. The conclusions and the next steps are provided in Chapter 6.

1.3 Intended Audience

The Airglow MONitor - network (AMON-net) system is developed by Department of Space Physics (DSP), Institute of Experimental Physics (IEP), Slovak Academy of Sciences (SAS) within the European Space Agency (ESA) / Plan for European Cooperating States (PECS) in Slovakia. The TN-TS provides scientific background for AMON-net development process. The Technical Note of Theoretical Study (TN-TS) is a deliverable to ESA team, that provides support to Cooperating States, for the review within the 2nd Milestone - Critical Design Review (CDR). It will be essentially used by DSP staff to continue in R&D activity SK2-09.

1.4 Acronyms and Abbreviations

AAC	AMON All-sky Camera
AMON	Airglow MONitor
AMON-ES	Airglow MONitor - Extended Station
AMON-net	Airglow MONitor - network
AGW	Atmospheric Gravity Waves
AURIC	Atmospheric Ultraviolet Radiance Integrated Code
CDR	Critical Design Review
DSP	Department of Space Physics
ESA	European Space Agency
GNSS	Global Navigation Satellite System
IEP	Institute of Experimental Physics
IGRF	International Geomagnetic Reference Field
LSO	Lomnicky Stit Observatory
MAITP-AE	Manufacturing, Assembly, Integration and Test Plan for the AMON-ES
PECS	Plan for European Cooperating States
R&D	Research & Development
SAS	Slovak Academy of Sciences
SK1-05	"Feasibility study to observe ionospheric disturbances by one pixel UV detector"
SK2-09	"Follow-up of feasibility study to observe ionospheric disturbances by airglow monitoring network (AMON-net)"
TEC	Total Electron Content
TN-SRS	Technical Note of System Requirements Specification
TID	Traveling Ionospheric Disturbances
TN1-AE	1st Technical Note of AMON-ES
TN-TS	Technical Note of Theoretical Study

1.5 References

[1] M. Putis, P. Bobik, and S. Mackovjak. Method for analysis of the effect of geomagnetic disturbances on UV airglow intensity. *Earth and Space Science*, 5(11):790–800, October 2018.

[2] Š. Mackovjak, P. Bobík, J. Baláž, I. Strhárský, M. Putiš, and P. Gorodetzky. Airglow monitoring by one-pixel detector. *Nuclear Instruments and Methods in Physics Research A*, 922:150–156, April 2019.

[3] Wikipedia. Ionosphere at Wikipedia, available at. `https://en.wikipedia.org/wiki/Ionosphere`, (accessed June 10, 2019).

[4] R. F. Pfaff. The Near-Earth Plasma Environment. *Space Sci. Rev.*, 168:23–112, June 2012.

[5] V. Y. Khomich, A. I. Semenov, and N. N. Shefov. *Airglow as an Indicator of Upper Atmospheric Structure and Dynamics*. Springer-Verlag, 2008.

[6] R. W. Eastes, W. E. McClintock, A. G. Burns, D. N. Anderson, L. Andersson, M. Codrescu, J. T. Correira, R. E. Daniell, S. L. England, J. S. Evans, J. Harvey, A. Krywonos, J. D. Lumpe, A. D. Richmond, D. W. Rusch, O. Siegmund, S. C. Solomon, D. J. Strickland, T. N. Woods, A. Aksnes, S. A. Budzien, K. F. Dymond, F. G. Eparvier, C. R. Martinis, and J. Oberheide. The Global-Scale Observations of the Limb and Disk (GOLD) Mission. *Space Sci. Rev.*, 212:383–408, October 2017.

[7] T. J. Immel, S. L. England, S. B. Mende, R. A. Heelis, C. R. Englert, J. Edelstein, H. U. Frey, E. J. Korpela, E. R. Taylor, W. W. Craig, S. E. Harris, M. Bester, G. S. Bust, G. Crowley, J. M. Forbes, J.-C. Gérard, J. M. Harlander, J. D. Huba, B. Hubert, F. Kamalabadi, J. J. Makela, A. I. Maute, R. R. Meier, C. Raftery, P. Rochus, O. H. W. Siegmund, A. W. Stephan, G. R. Swenson, S. Frey, D. L. Hysell, A. Saito, K. A. Rider, and M. M. Sirk. The Ionospheric Connection Explorer Mission: Mission Goals and Design. *Space Sci. Rev.*, 214:13, February 2018.

[8] J. Grobowsky / NASA GSFC. Terrestrial Atmosphere Processes, available at. `https://www.nasa.gov/mission_pages/sunearth/science/itm-processes.html`, (accessed June 10, 2019).

[9] Christian von Savigny. Airglow in the earth atmosphere: basic characteristics and excitation mechanisms. *ChemTexts*, 3(4):14, Oct 2017.

[10] Samantha Cristoforetti / ESA. ISS-42 Starry Night, available at. `https://commons.wikimedia.org/wiki/File:ISS-42_Starry_Night_(2).jpg`, (accessed June 10, 2019).

[11] Lord Rayleigh and H. Spencer Jones. The Light of the Night-Sky: Analysis of the Intensity Variations at Three Stations. *Proceedings of the Royal Society of London Series A*, 151(872):22–55, Aug 1935.

[12] K. A. Deutsch and G. Hernandez. Long-term behavior of the OI 558 nm emission in the night sky and its aeronomical implications. *Journal of Geophysical Research (Space Physics)*, 108:1430, December 2003.

[13] Guiping Liu and Gordon G. Shepherd. An investigation of the solar cycle impact on the lower thermosphere o(1s) nightglow emission as observed by windii/uars. *Advances in Space Research*, 42(5):933 – 938, 2008.

[14] Iain M. Reid, Andrew J. Spargo, and Jonathan M. Woithe. Seasonal variations of the nighttime O (1S) and OH (8-3) airglow intensity at Adelaide, Australia. *Journal of Geophysical Research: Atmospheres*, 119(11):6991–7013, 2014.

[15] G. G. Shepherd, Y.-M. Cho, G. Liu, M. G. Shepherd, and R. G. Roble. Airglow variability in the context of the global mesospheric circulation. *Journal of Atmospheric and Solar-Terrestrial Physics*, 68:2000–2011, December 2006.

[16] Guiping Liu, Gordon G. Shepherd, and Raymond G. Roble. Seasonal variations of the nighttime o(1s) and oh airglow emission rates at mid-to-high latitudes in the context of the large-scale circulation. *Journal of Geophysical Research: Space Physics*, 113(A6), 2008.

[17] NASA/GSFC. Upper Atmosphere Research Satellite. `http://umpgal.gsfc.nasa.gov`, (accessed June 10, 2019).

[18] W. D. Gonzalez, J. A. Joselyn, Y. Kamide, H. W. Kroehl, G. Rostoker, B. T. Tsurutani, and V. M. Vasyliunas. What is a geomagnetic storm? *Journal of Geophysical Research: Space Physics*, 99(A4):5771–5792, 1994.

[19] S. M. Silverman. Night Airglow Phenomenology. *Space Sci. Rev.*, 11:341–379, October 1970.

[20] L. A. Leonovich, A. V. Mikhalev, and V. A. Leonovich. The 557.7 and 630-nm atomic oxygen midlatitude airglow variations associated with geomagnetic activity. *Atmospheric and Oceanic Optics*, 24(4):396, Aug 2011.

[21] Jonathan J. Makela, Brian J. Harding, John W. Meriwether, Rafael Mesquita, Samuel Sanders, Aaron J. Ridley, Michael W. Castellez, Marco Ciocca, Gregory D. Earle, Nathaniel A. Frissell, Donald L. Hampton, Andrew J. Gerrard, John Noto, and Carlos R. Martinis. Storm time response of the midlatitude thermosphere: Observations from a network of fabry-perot interferometers. *Journal of Geophysical Research: Space Physics*, 119(8):6758–6773, 2014.

[22] T. Bag, Vir Singh, and M.V. Sunil Krishna. Study of atomic oxygen greenline dayglow emission in thermosphere during geomagnetic storm conditions. *Advances in Space Research*, 59(1):302 – 310, 2017.

[23] A. Saito, M. Nishimura, M. Yamamoto, S. Fukao, M. Kubota, K. Shiokawa, Y. Otsuka, T. Tsugawa, T. Ogawa, M. Ishii, T. Sakanoi, and S. Miyazaki. Traveling ionospheric disturbances detected in the front campaign. *Geophysical Research Letters*, 28(4):689–692, 2001.

[24] J.S. Haase, T. Dautermann, M.J. Taylor, N. Chapagain, E. Calais, and D. Pautet. Propagation of plasma bubbles observed in brazil from gps and airglow data. *Advances in Space Research*, 47(10):1758 – 1776, 2011. GNSS Remote Sensing-2.

[25] IGY. International Geophysical Year - Airglow data. `ftp://ftp.ngdc.noaa.gov/STP/SOLAR_DATA/SOLAR_PHENOMENON/AIRGLOW_IGY/`, (accessed June 10, 2019).

[26] G. G. Didebulidze, L. N. Lomidze, N. B. Gudadze, A. D. Pataraya, and M. Todua. Long-term changes in the nightly behaviour of the oxygen red 630.0 nm line nightglow intensity and trends in the thermospheric meridional wind velocity. *International Journal of Remote Sensing*, 32(11):3093–3114, 2011.

[27] Maya Todua and Goderdzi Didebulidze. Cosmic factors influence on the inter-annual variations of the green 557.7 Nm line and red 630.0 Nm line nightglow intensities and their possible coupling with cloud covering at Abastumani (41.75°N, 42.82°E). *Acta Geophysica*, 62(2):381–399, Apr 2014.

[28] D.J. Strickland, J. Bishop, J.S. Evans, T. Majeed, P.M. Shen, R.J. Cox, R. Link, and R.E. Huffman. Atmospheric ultraviolet radiance integrated code (auric): theory, software architecture, inputs, and selected results. *Journal of Quantitative Spectroscopy and Radiative Transfer*, 62(6):689 – 742, 1999.

[29] J. BARTELS. The technique of scaling indices k and q of geomagnetic activity. *Ann. Intern. Geophys.*, 4:215–226, 1957.

[30] GFZ. Indices of Global Geomagnetic Activity. `https://www.gfz-potsdam.de/en/kp-index/`, (accessed June 10, 2019).

[31] Erwan Thébault, Christopher C. Finlay, Ciarán D. Beggan, Patrick Alken, Julien Aubert, Olivier Barrois, Francois Bertrand, Tatiana Bondar, Axel Boness, Laura Brocco, Elisabeth Canet, Aude Chambodut, Arnaud Chulliat, Pierdavide Coïsson, François Civet, Aimin Du, Alexandre Fournier, Isabelle Fratter, Nicolas Gillet, Brian Hamilton, Mohamed Hamoudi, Gauthier Hulot, Thomas Jager, Monika Korte, Weijia Kuang, Xavier Lalanne, Benoit Langlais, Jean-Michel Léger, Vincent Lesur, Frank J. Lowes, Susan Macmillan, Mioara Mandea, Chandrasekharan Manoj, Stefan Maus, Nils Olsen, Valeriy Petrov, Victoria Ridley, Martin Rother, Terence J. Sabaka, Diana Saturnino, Reyko Schachtschneider, Olivier Sirol, Andrew Tangborn, Alan Thomson, Lars Tøffner-Clausen, Pierre Vigneron, Ingo Wardinski, and Tatiana Zvereva. International geomagnetic reference field: the 12th generation. *Earth, Planets and Space*, 67(1):79, May 2015.

[32] N. A. Tsyganenko. A model of the near magnetosphere with a dawn-dusk asymmetry 1. Mathematical structure. *Journal of Geophysical Research (Space Physics)*, 107:1179, August 2002.

[33] Tsyganenko. Modeling the Earth's Magnetosphere Using Spacecraft Magnetometer Data. `http://geo.phys.spbu.ru/~tsyganenko/modeling.html`, (accessed June 10, 2019).

[34] Wonhyeong Yi and Jiyoung Kim. Comparison of planetary and local geomagnetic disturbance indices: Operational implications. *Journal of Atmospheric and Solar-Terrestrial Physics*, 178:1 – 6, 2018.

Chapter 2

Summary of SK1-05 activity

During the previous activity "Feasibility study to observe ionospheric disturbances by one pixel UV detector" (SK1-05), we have concentrated on the evaluation the global maps of airglow production. The maps were created for empirical input parameters and for input parameters characteristic for non and very disturbed magnetosphere. The analysis of airglow maps demonstrated that the airglow production at higher latitudes is more sensitive to the magnetospheric disturbances. On the other hand, at high latitudes, the airglow observations could be hampered by auroral lights. This led to selection of optimal points for observation of airglow changes induced by geomagnetic activity at auroral ovals positions for very disturbed magnetosphere. This selection was a compromise between as most high latitude position as possible and reasonably equator-ward position to not be influenced by auroral lights. For selected positions the airglow production was evaluated. The method called Slope method was developed to analyze and quantify average effect of geomagnetic disturbances on airglow production data represented by simulated time series. Based on realized simulations and following analysis results, it was concluded that airglow production decreases during the magnetospheric disturbances by tens percents. Therefore the UV airglow intensity variation driven by geomagnetic storms might be clearly visible on the selected locations. The details of this study were also published in [1].

We have also investigated all main atmospheric conditions and their influence to the transmitting UV light from the top of the atmosphere to the ground. The conclusion was, that according verified model of radiative transfer - libRadtran, the variations of the atmospheric conditions should not preclude the detection of ionospheric disturbances by observation of airglow intensity. However, there was a one exception - presence of clouds - that is needed to be seriously monitored. To estimate the portion of measurements that might be possible during the year, we have assessed clear sky probability for the selected observational sites. Assuming influence of atmosphere we have theoretically justified possibility to observe geomagnetic disturbances by one pixel UV detector for airglow monitoring (AMON).

The theoretical assumptions tried to be confirmed by first measurements of 4 Airglow MONitor (AMON) instruments. Detailed reduction of the data was performed while the data affected by the presence of the light from the Sun, Moon, Milky Way and bright stars were excluded. We employed also data of cloud coverage to select only these data that were taken during cloudless (clear sky) conditions. These UV airglow intensity measurements were investigated

and possible connections to the ionospheric disturbances caused by geomagnetic storms were indicated in 3 periods. Despite of strong improvements in the data quality by measurements in Mexico and La Palma sites, the measurement period in years 2017 - 2018 and hence data therein did not contain enough geomagnetic active events. Quantification of airglow production sensitivity to the ionospheric disturbances caused by geomagnetic storms was due to this obstacle not established. Nevertheless, all of the results demonstrated that AMON might be able to detect variations in airglow intensity and so disturbances in the ionosphere. The details of this analysis were published in [2].

The SK1-05 activity with the title "Feasibility study to observe ionospheric disturbances by one pixel UV detector" was enclosed with the statement that the follow-up activity is required to demonstrate if network of AMON instruments (AMON-net) is able to detect and monitor ionospheric disturbances. This effort is described in the delivered reports of SK3-02 activity i.e. Technical Note of System Requirements Specification (TN-SRS), Manufacturing, Assembly, Integration and Test Plan for the AMON-ES (MAITP-AE), and 1st Technical Note of AMON-ES (TN1-AE). In this report TN-TS, theoretical background, that is needed for other reports, is provided.

Chapter 3

Theoretical background for AMON-net

3.1 The Earth's upper atmosphere

The Earth's atmosphere can be divided into five main layers (Figure 3.1) based on the vertical temperature distribution (troposphere, stratosphere, mesosphere, thermosphere and exosphere) or into two categories based on the composition (lower atmosphere - homosphere and upper atmosphere - heterosphere). The boundary of the lower and upper atmosphere is near 86 km while the relative percentage of the major components N_2 and O_2 remain constant bellow this boundary and the composition is significantly changed by EUV solar radiation above it.

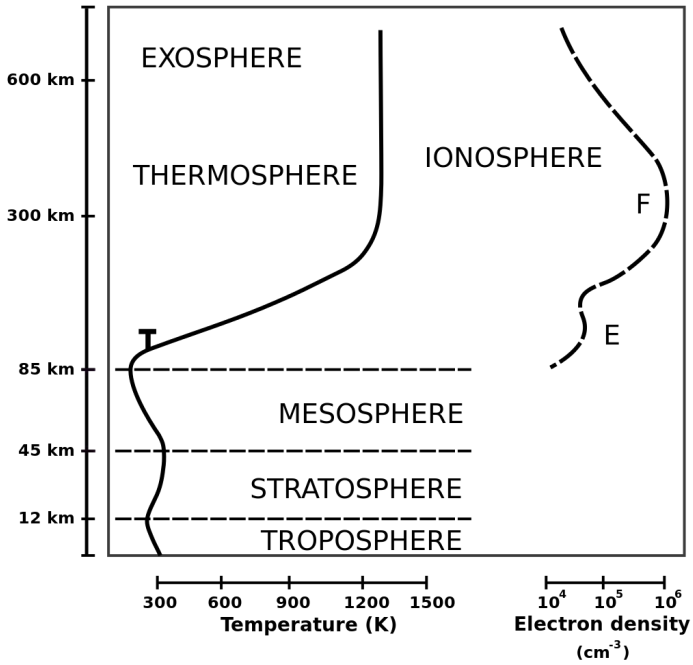

Figure 3.1: The simplified classification of the Earth's atmosphere. The upper atmosphere consists of the neutral part - thermosphere and the ionized part - ionosphere [3].

The main process by which the upper atmosphere absorbs the EUV solar radiation is photo-dissociation. The oxygen molecules (O_2) are the primary molecules that dissociates to atomic oxygen when they are struck by photons with wavelength less then 242 nm:

$$O_2 + h\nu(\lambda{<}242 \text{ nm}) \longrightarrow O + O + \text{energy}.$$

The creation of atomic oxygen is crucial as it is the main constituent in photo-ionization mechanism that creates ionosphere:

$$O + h\nu \longrightarrow O^+ + e^-.$$

The concentration of atomic oxygen and other constituents per unit volume and their variation in the upper atmosphere affect the ionosphere in two ways. First, they determine the amount of neutral gas available for photo-ionization, and second, they determine to what depth the solar EUV radiation might penetrate i.e. in which altitude the photo-ionization occurs. Therefore, the densities of the neutral gasses and plasma (ions and electrons) is influenced by various phenomena affected them from above and also from bellow (Figure 3.2).

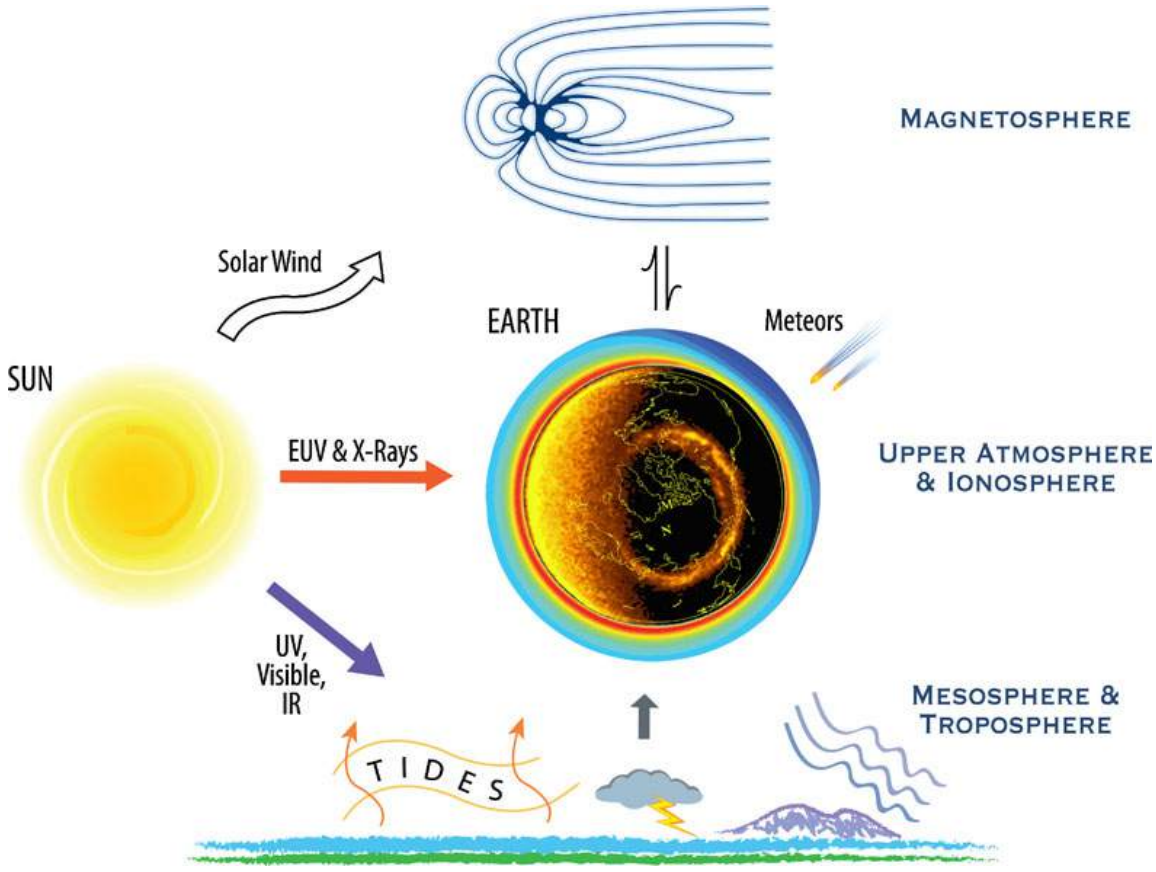

Figure 3.2: The various phenomena that affect upper atmosphere from above (solar radiation, solar wind and effects in magnetosphere) and from bellow (effects as lightning, tides, planetary waves, and atmospheric gravity waves in mesosphere and troposphere) [4].

The main path how the Sun directly influences the upper atmosphere via EUV radiation is photo-ionization as it is described above. Another related path is via heating of neutral atmosphere, which results in its expansion. Both processes therefore generate significant variations in the upper atmosphere as a consequence of the solar cycle, position of the Earth against the Sun during the year and throughout the day. The significance of the solar radiation variation to the creation of ionosphere is illustrated in Figure 3.3.

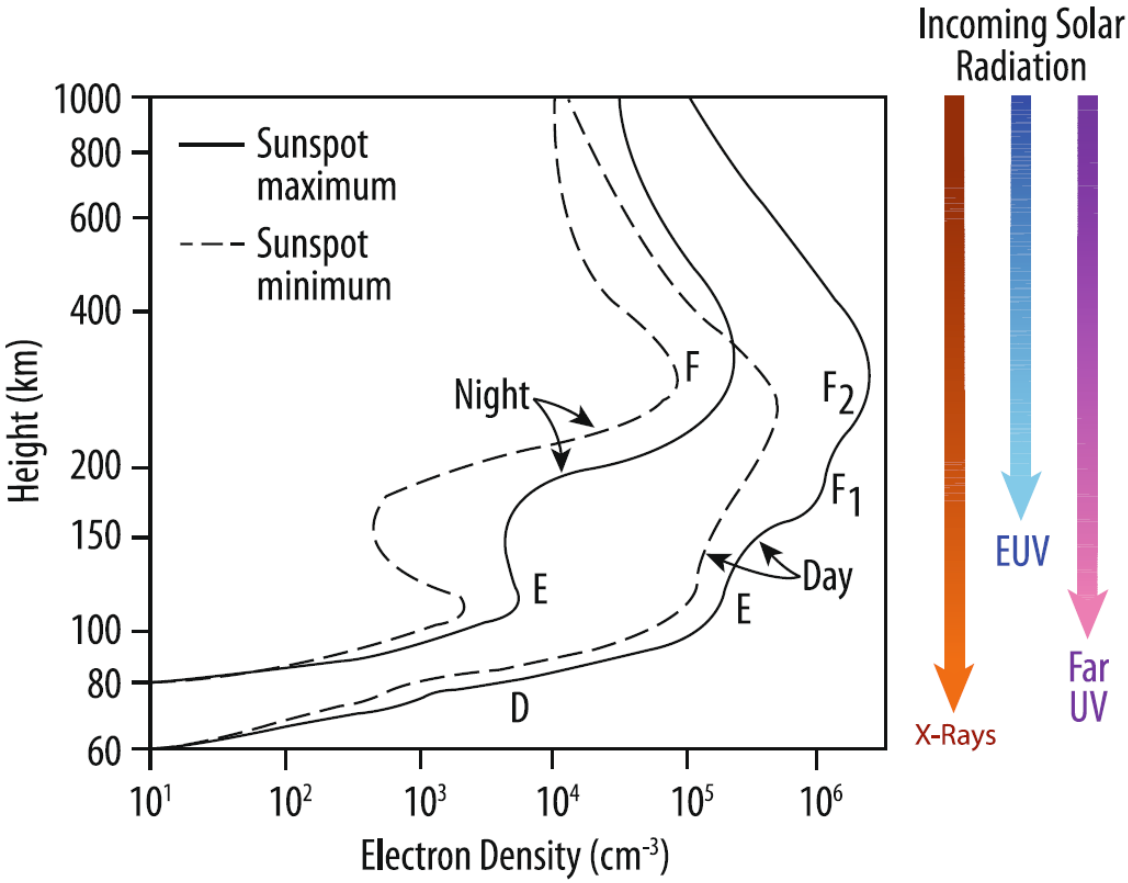

Figure 3.3: The representative ionosphere profiles for day and night at solar minimum and maximum at a mid-latitude location. The colored arrows represent the approximate penetration depth of solar radiation [4].

The another path how the Sun influences the upper atmosphere (Figure 3.2) is via the solar wind processes, including plasma flow with embedded interplanetary magnetic fields. They interact with the magnetosphere and drive large scale electric fields, currents, and energetic particles that subsequently interact with the underlying upper atmosphere mainly at high latitudes. Although it could influence all latitudes during periods of geomagnetic storms. The influence of other outer sources as cosmic rays and meteors are not so significant.

The sketch in Figure 3.2 present that the upper atmosphere is also influenced by energy and momentum from bellow, namely from electrical discharges (lightning, sprites, etc.) as well as upward-propagating tides, planetary waves, and atmospheric gravity waves. All of these sources might be significant for short-therm variations of the constituents' concentration in

the upper atmosphere. Indeed, the distribution of ions within the ionosphere is controlled to a large extent by the distributions of the neutral gas constituents.

All of the sources and phenomena mentioned above create multitude of variations and instabilities in the upper atmosphere. The complexity of these processes is indicated in Figure 3.4 and are described in details in [4], [5], [6], [7]. In this section, we tried to present that the charged part of upper atmosphere - ionosphere and the neutral part - thermosphere are very closely connected. In the next section, it is presented that an airglow formed in thermosphere can be effectively used for monitoring of upper atmosphere dynamics.

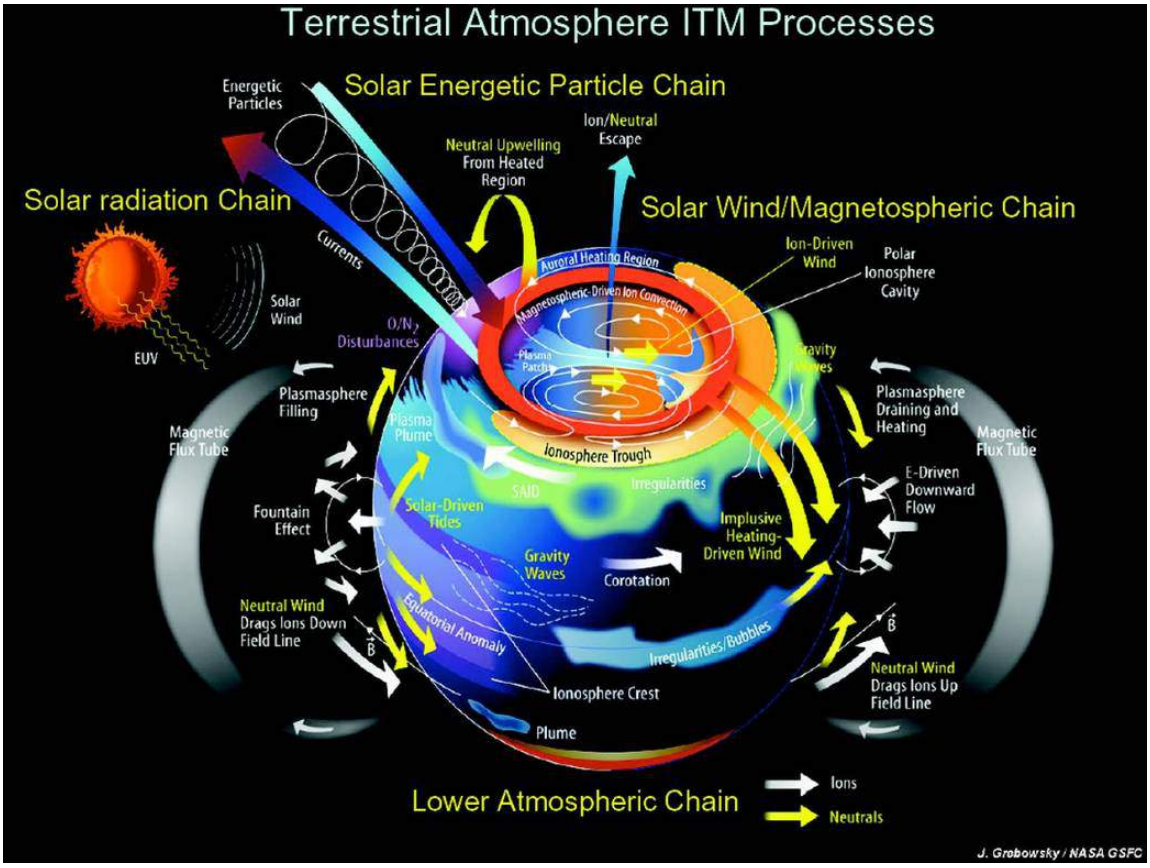

Figure 3.4: The indication of complexity of the Earth's upper atmosphere (ionosphere-thermosphere-mesosphere (ITM)) with the multitude of variations and instabilities [8].

3.2 Airglow

Airglow is a non-thermal emission of light originated from excited atomic or molecular states. The source of the excitation is provided directly or indirectly by solar electromagnetic radiation. Depending on solar elevation the airglow can be categorized as dayglow, twilightglow and nightglow [9]. Dayglow emission is the brightest but its observation is very difficult due to present of direct and scattered light from the Sun. Therefore, every time the term airglow is used, the nightglow (solar zenith angle is higher than 110°) is considered. The particular process responsible for airglow emission and amount of this emission is mainly dependent on the

composition and concentrations of neutral constituents in upper atmosphere. Their vertical profiles are displayed in Figure 3.5. So the airglow production is increasing with the increase of density. But if the density is to high, the excited atom or molecule may be quenched by collisions. This is an explanation why airglow is the upper atmosphere phenomenon and does not occur in lower atmosphere (collisional relaxation is too efficient at the lower altitudes.)

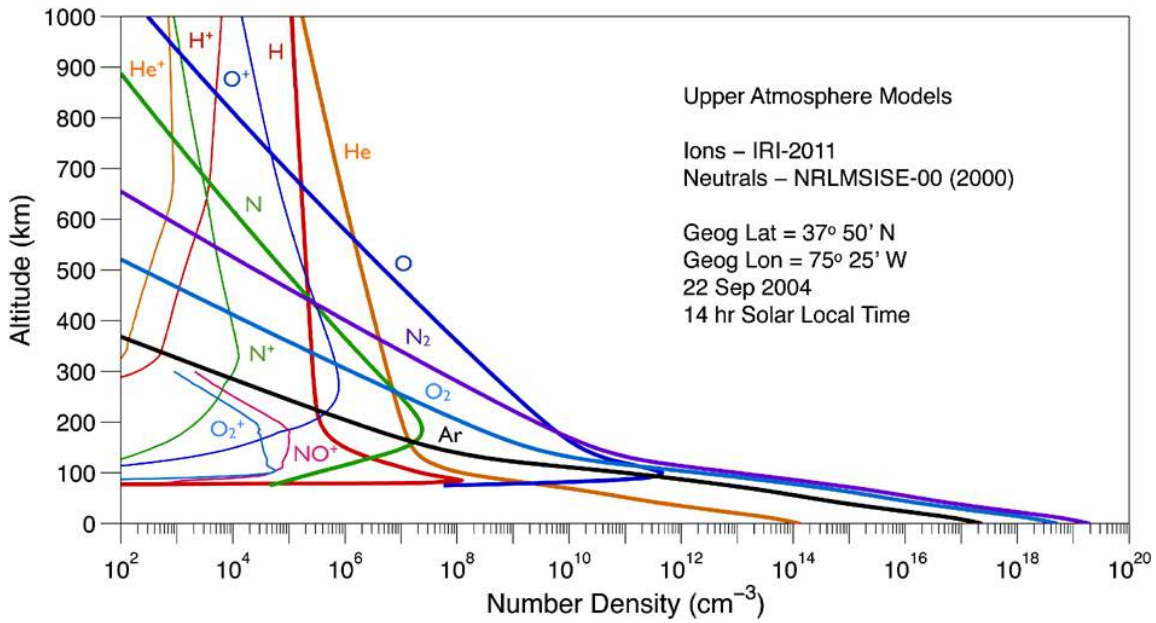

Figure 3.5: The vertical profiles of neutral and ionic constituents in the upper atmosphere [4].

The most prominent airglow layers are represented by enhanced emission in specific wavelengths (Figure 3.6). Here are the main airglow emissions [5]:

- Emission of the OI 630.0 nm (red airglow) with the peak at altitude 250–300 km. The intensity is sensitive to the ionospheric F region height (as it is situated bellow its peak) and is proportional to its electron density. The disociative recombination is the most significant process that contributes to the emission:

$$\begin{aligned} O^+ + O_2 &\longrightarrow {O_2}^+ + O, \\ {O_2}^+ + e^- &\longrightarrow O^*(^1D) + O, \\ O^*(^1D) &\longrightarrow O(^3P_2) + h\nu(\lambda{=}630.0\text{ nm}). \end{aligned}$$

- Emission of the OI 557.7 nm (green airglow) with the peak at altitude $\approx$ 97 km. The emission can be easily recognised by detectors in visible band (Figure 3.6). The Barth's mechanism is the most important source of excited atomic oxygen:

$$\begin{aligned} O + O + M &\longrightarrow {O_2}^* + M, \\ {O_2}^* + O &\longrightarrow O_2 + O^*(^1S), \\ O^*(^1S) &\longrightarrow O^*(^1D_2) + h\nu(\lambda{=}557.7\text{ nm}). \end{aligned}$$

- Emission of hydroxyl molecule OH in IR range with the peak at altitude 85–95 km. It is not originated from electronic transitions, but from vibrational and rotational transitions only. The band system known as Meinel Hydroxyl Band consists of high number of spectral lines with wavelengths 700–1800 nm. Vibrationally excited OH is produced near the mesopause via the exothermic reaction:

$$\mathrm{H} + \mathrm{O_3} \longrightarrow \mathrm{OH^*} + \mathrm{O_2},$$
$$\mathrm{OH^*} \longrightarrow \mathrm{OH} + \mathrm{h}\nu (\lambda \approx 700\text{–}1800\ \mathrm{nm}).$$

- Emission of molecular oxygen O_2 in UV range with the peak at altitude 90–100 km. According electronic transitions responsible for UV emission the band systems are defined. The most intensive band systems are Herzberg I, Herzberg II, Herzberg III, and Chamberlain system.

$$\mathrm{O} + \mathrm{O} + \mathrm{M} \longrightarrow \mathrm{O_2^*} + \mathrm{M},$$
$$\mathrm{O_2^*} \longrightarrow \mathrm{O_2} + \mathrm{h}\nu (\lambda \approx 300\text{–}400\ \mathrm{nm}).$$

There is a high number of other airglow emissions that could be observed by high-sensitive spectrometers. The most intensive emissions can be effectively observed by photometers and imagers with narrow band filters. It is important to emphasise that the airglow is emitted from relative thin layers ($\approx$ 10 km). So by measuring the intensity in different wavelengths, different layers in upper atmosphere can be monitored (Figure 3.6).

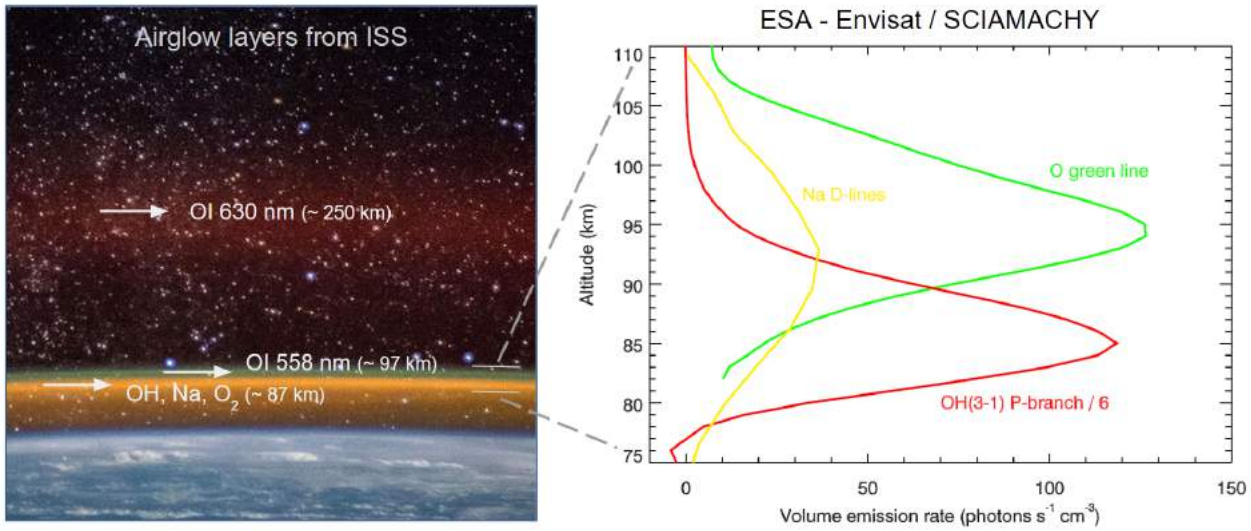

Figure 3.6: Left: The airglow layers captured by ESA astronaut Samantha Cristoforetti from ISS with denominated main emissions [10]. Right: Volume emission rate profiles retrieved from monthly and zonally averaged satellite observations for March 2009 with the SCIAMACHY instrument on Envisat (ESA). Note that the OH(3-1) (1520 nm) emission rates are divided by 6 to improve presentation [9].

The knowledge of the mentioned main emissions was used in the design process of AMON All-sky Camera (AAC) that is part of Airglow MONitor - Extended Station (AMON-ES) described in 1st Technical Note of AMON-ES (TN1-AE).

3.3 Detection of ionospheric disturbances by airglow monitoring

One of the core tasks of the SK2-09 activity is to answer the question if it is feasible to monitor ionospheric disturbances by airglow monitoring. As it was presented in Section 3.1, thermosphere and ionosphere are closely linked and there are many of phenomena that cause disturbances in upper atmosphere. Here we would like to provide a brief overview of the different published studies that were dedicated to detection of these various disturbances by observation of airglow.

The longest detected variation is connected to the 11-years solar cycle. The correlation between the airglow emission of green line (557.7 nm) with sunspot area was revealed in 1935 [11]. The connection of solar activity, expressed by solar flux F10.7 (f = 2800 Mhz) was confirmed by extensive studies [12] [13] [14]. They provide clear evidence of the green line intensity is maximal during the maximum of solar cycle (Figure 3.7). This correlation was demonstrated also in our analysis in Chapter 4.

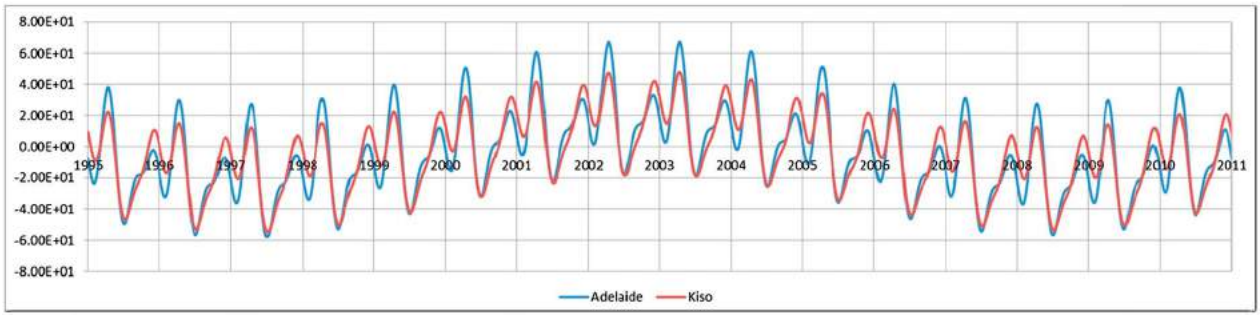

Figure 3.7: The fitted relative variation of airglow green line observed at Adelaide (Australia, 35° S). The data from Kiso (Japan, 35° N) measured in years 1979–1995 are over-plotted for the corresponding part of solar cycle. The maximum of airglow intensity occurs during maximum of solar cycle 23 in 2002 and the minimum is in years 1997 and 2008. [14].

The Figure 3.7 present also other significant variations within the year (annual oscillation and semi-annual oscillation) that is associated with the yearly tilt and rotation of the Earth around the Sun and also with the dynamics in the whole atmosphere, mainly driven by atmospheric tides. The amplitude and maximum of period are different for different locations. Authors in [15] [16] used UARS/WINDII [17] space based observations of green line (557,7 nm) in years 1991–1997 to present airglow variations during the year and also during the local time (diurnal variation) for different latitudes (Figure 3.8). The authors concluded that for equatorial region semi-annual variation has maxima at equinoxes and diurnal variation has maximum in the evening. For the mid-latitude regions, the annual variation is dominant and has maximum in autumn on the north hemisphere and in spring on the south hemisphere. The diurnal variation has maximum in the morning.

There are also shorter and not periodic variations in the upper atmosphere. They are caused by consequences of space weather and also by tropospheric weather. The occurrence of geomagnetic storms is a well known consequence of the space weather driven by solar activity [18].

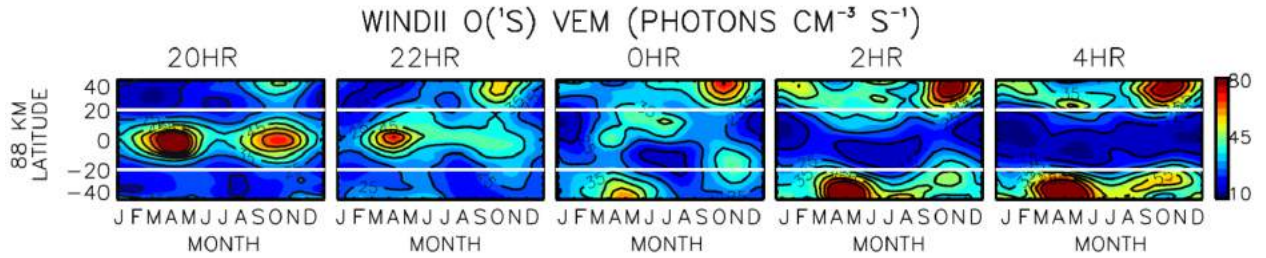

Figure 3.8: The seasonal variations of the green airglow as observed by UARS/WINDII for altitude 88 km and local times from 20 to 04 h [16].

The influence of geomagnetic storms have been observed in the airglow intensity measurements since the mid-twentieth century [19]. During the geomagnetic storm the density distribution of the ions and neutral constituents in upper atmosphere vary dramatically. A such variations might have signatures in the airglow emission [20] [21] [22]. We are study the role of geomagnetic field in more details in Chapter 5.

The tropospheric weather and space weather might induce Atmospheric Gravity Waves (AGW) that could caused significant variations in thermosphere-ionosphere system. In general, apart from singular and local events such as earthquakes, there are two main typed of AGW in mid and low-latitudes [4]:

- upwards-propagating gravity waves that originate in lower atmosphere as a product of orography, thunderstorms, and other tropospheric energy sources,
- horizontally-propagating gravity waves generated at high latitudes, for example by aurora processes, that subsequently propagate eqautorword.

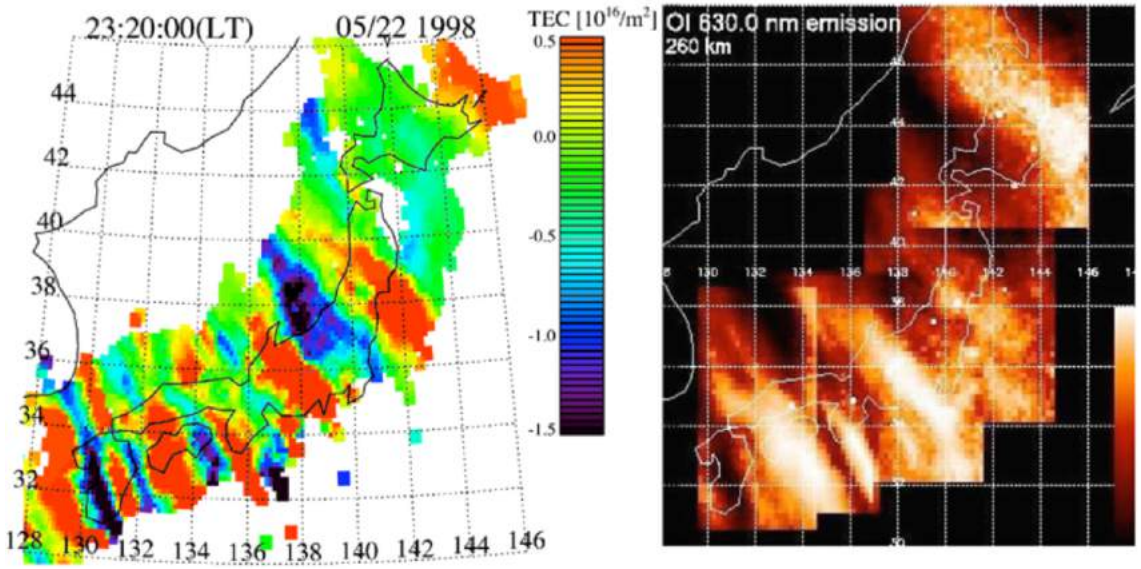

Figure 3.9: The simultaneous observation of Traveling Ionospheric Disturbances (TID) by measurement of Total Electron Content (TEC) with GPS receivers *(left)* and by measurements of red airglow (630.0 nm) with the all sky imagers *(right)* [23].

The motion of neutral gasses associated to gravity waves set also the charged particles in ionosphere to the motion. This motion is observed as Traveling Ionospheric Disturbances (TID). The TID can be effectively observed by the Global Navigation Satellite System (GNSS) receivers and also by the airglow imagers. Such simultaneous measurements were reported by [23] over Japan (Figure 3.9).

The gravity waves could act as a source of perturbation for initiating plasma bubble events in ionosphere. This plasma depletion might be also detected simultaneously by monitoring airglow and Total Electron Content (TEC) (Figure 3.10).

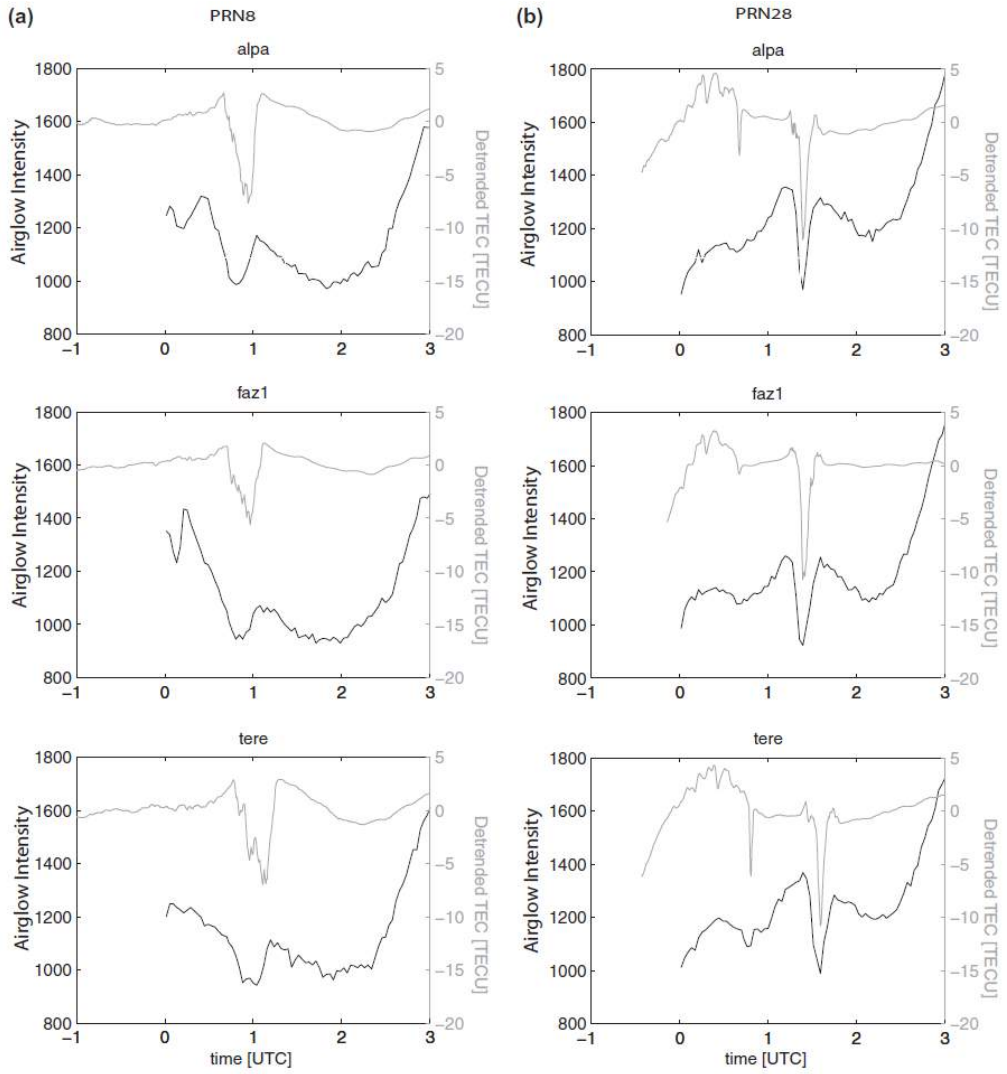

Figure 3.10: The extracted intensity from the image of red airglow (630.0 nm) and measured Total Electron Content (TEC) by using signals from two GPS satellites (PRN8 and PRN28) on three observational locations (alpa, faz1, tere) in Brazil. For the satellite PRN28 the airglow depletion occurred exactly in the same time as drop in measured TEC [24].

There are plenty of other disturbances that could be monitored by airglow observations. The overview of the published studies will be extended if it fill be beneficial for AMON-ES and AMON-net operation and data analysis.

Chapter 4

Airglow historical data

The analysis within SK1-05 activity was limited by the amount of the airglow measurements. Now we have the data from two years of AMON measurement (Figure 4.1) but only in UV range. The amount of the valuable airglow data is rapidly increasing by operation of AMON-ES (see TN1-AE) but probably we will be not able to detect many events like geomagnetic storms in the following years as the Sun is approaching to the minimum of its activity. Therefore we tried to find some archives of airglow data to extend our analysis.

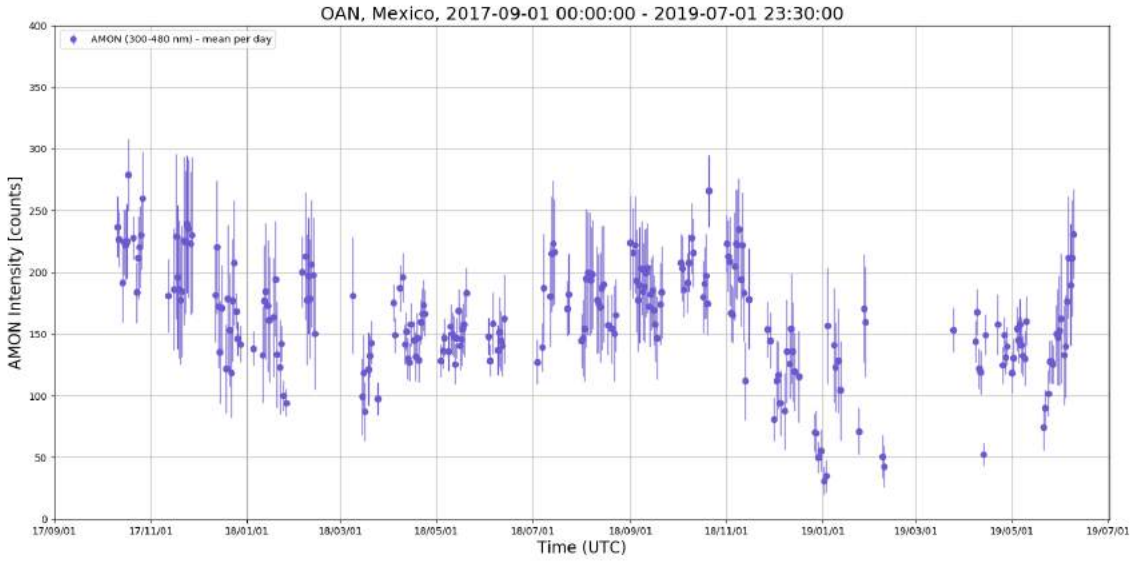

Figure 4.1: The mean values with their standard deviations of AMON measurements at OAN (Mexico) for period September 2017 - June 2019. The AMON was pointed to the zenith. Data contaminated by influence of Sun, Moon and clouds are excluded.

The first source of the airglow historical data is archive available on [25]. There are data from 28 locations around the globe that participated on activities within International Geophysical year in 1957 - 1958. The airglow data from Lomnicky Stit Observatory (LSO) in Slovakia are also available (Figure 4.2). The data will be compared with available space weather indexes and their potential profitability will be considered.

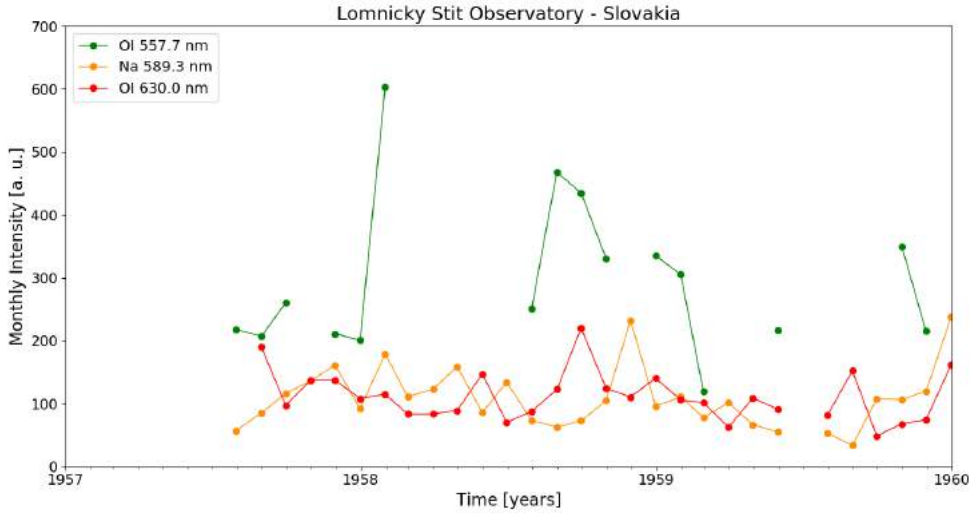

Figure 4.2: The monthly means of airglow photometric data observed at LSO in years 1957–1959.

We have also obtained calibrated photometric data of green airglow (557.7 nm) red airglow (630 nm) and OH airglow (900 - 1 055 nm) measured at Abastumani (Georgia) in years 1975 - 1993 [26] [27]. Such long duration measurements are useful for study of long term variations of airglow production influenced by solar cycle (Figure 4.3) or by season (Figure 4.4), as it is described in Chapter 3.

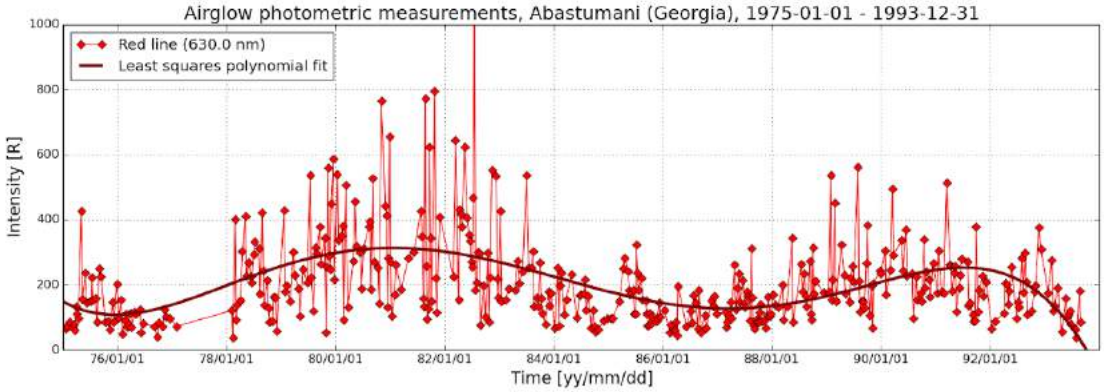

Figure 4.3: The time series of airglow red line intensities averaged per week. They were measured at Abastumani (Georgia) from 1 January 1975 to 31 December 1992. The maximum of the 21st and 22nd solar cycle occurred in the years 1980 and 1991, respectively.

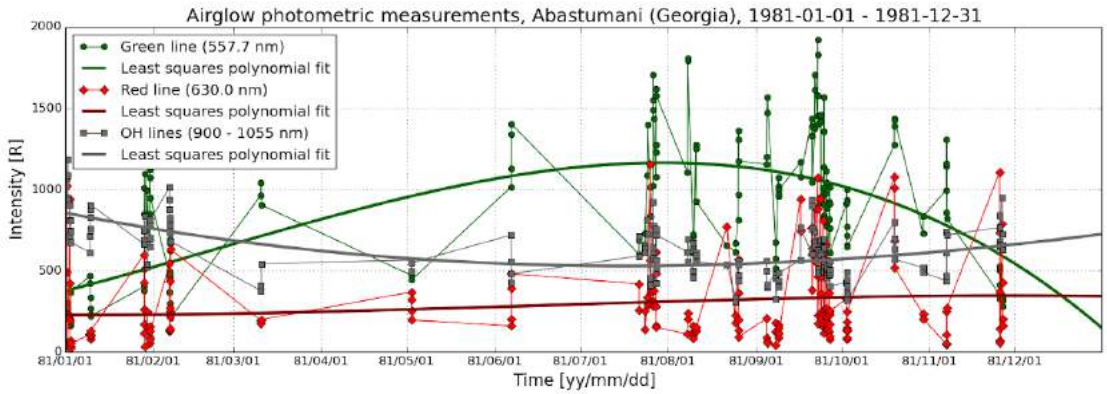

Figure 4.4: The time series of airglow lines intensities averaged per hour. They were measured at Abastumani (Georgia) from 1 January to 31 December 1981. The intensities of green line (557.7 nm) fitted by least square polynomial fit indicate seasonal variation with the maximum in the autumn. The similar behaviour was observed also for other years.

Since, such long term variations are not a primary objective of our activity, we have focused on the variations that could be caused by geomagnetic storms and take usually several days. Unfortunately, the weather conditions at Abastumani (Georgia) location are not so satisfactory as locations of AMON detector (OAN in Mexico or ORM at La Palma). There were usually 40 - 50 cloudless night periods without Moonlight contamination at Abastumani (Georgia) within one year. At AMON locations (OAN or ORM) the number of cloudless night periods without moonlight is roughly 3 times higher. For this reason, the Slope method (developed within SK1-05 activity) works not very well for data from Georgia. It is due to lack of consecutive days with measurements. So we tried to make correlation between measured intensities of airglow lines (557.7, 630.0 and 900 - 1055 nm) and Dst index. The results are displayed in Figure 4.5.

The correlation plots displayed in Figure 4.5 reflect that the there is very low direct correlation between airglow lines intensities and Dst index. But this could be a consequence of the fact that the airglow lines intensities are continuously affected by various phenomena that occurred in the Earth's upper atmosphere, not just by geomagnetic activity. When we want to find straightforward correlation between geomagnetic storms and variations in airglow intensities we need to understand influence of all other phenomena.

The upper atmosphere is rather variable than constant also during quiet magnetosphere periods. The example is displayed in the Figure 4.6. The intensities of airglow red line (630.0 nm) that is produced at altitude $\sim$ 220–260 km are stable but the intensities of airglow green line (557.7 nm) and OH lines (900–1055 nm) that are produced at altitude 80–100 km are significantly disturbed during period of several days. The study of such events will continue during whole SK2-09 activity.

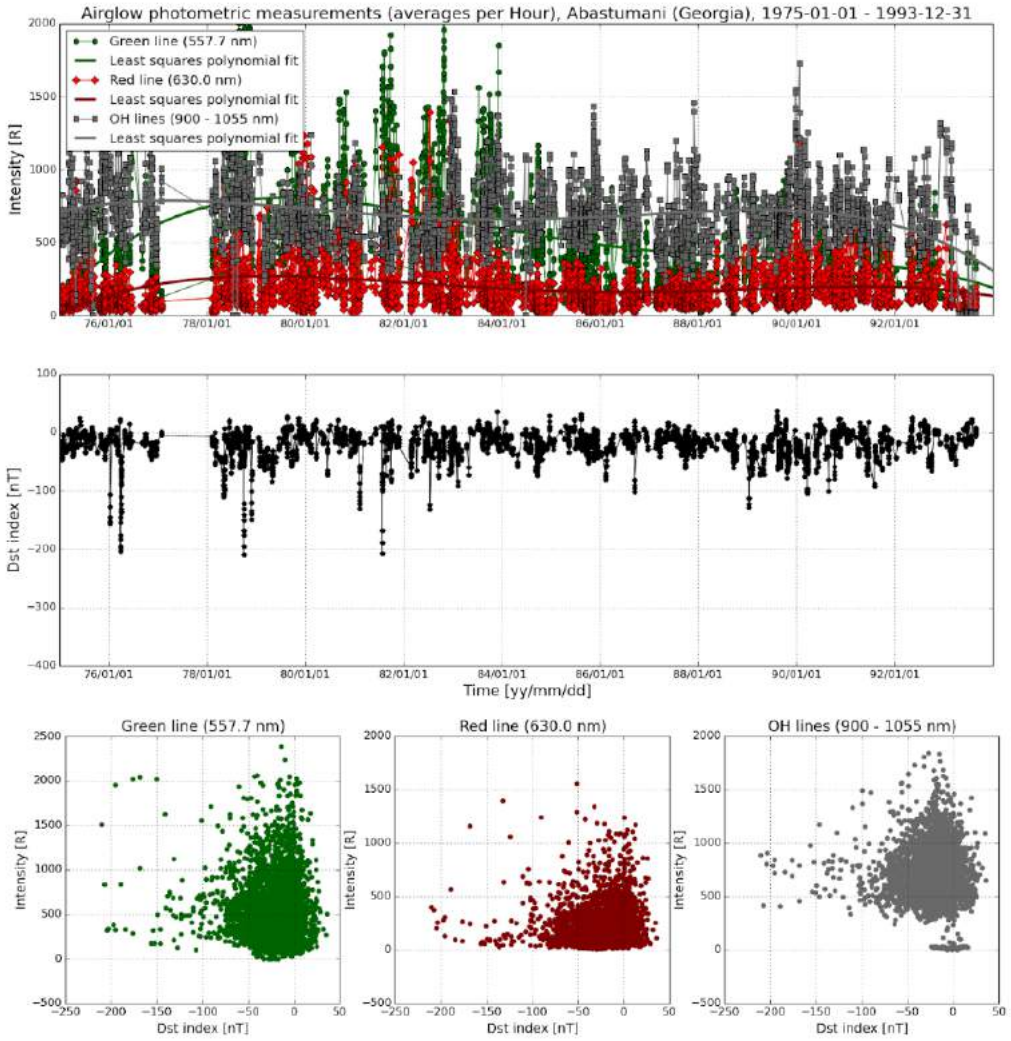

Figure 4.5: Top: The time series of airglow lines intensities averaged per hour. They were measured at Abastumani (Georgia) from 1 January 1975 to 31 December 1993. Middle: The geomagnetic activity expressed by Dst index for the respective hours of airglow measurements. Bottom: Correlation plots between Dst index and particular airglow lines.

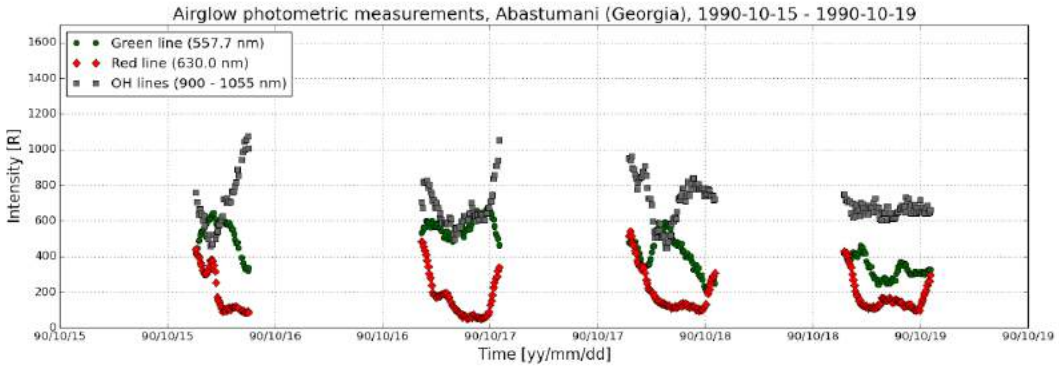

Figure 4.6: The time series of airglow lines (557.7, 630.0 and 900 - 1055 nm) intensities measured at Abastumani (Georgia) in period 15 - 19 October 1990.

Chapter 5

Local geomagnetic field dynamics

As it was mentioned in Chapter 3.1, solar wind and processes in magnetosphere play the role in formation of airglow mainly for the high latitudes. However, during the geomagnetic storm periods, airglow production at all latitudes might be affected. This was studied within the SK1-05 activity, where we focused on airglow production response to disturbances caused by geomagnetic storms. The airglow production results were evaluated in Atmospheric Ultraviolet Radiance Integrated Code (AURIC) model [28]. Generally speaking, AURIC use a global Ap index of geomagnetic activity as inputs for evaluation of airglow local response to geomagnetic storms. Global Ap index is derived from Kp index [29] [30]. Kp index is planetary index averaged from K indexes whose quantifies disturbance in the horizontal component of geomagnetic field. K indexes are measured at 13 stations covering mostly middle latitudes from 38°12' N Fredericksburg (USA) till Lerwick at 60°08' N (Scotland) in northern hemisphere and from Canbera (Australia) with latitude 35°18' S till Eyrewell (New Zealand) at 43°25' S in southern hemisphere [30].

The aim of realized and following research is the estimation of global geomagnetic indexes influence to airglow production in comparison with the locally measured geomagnetic field influence. Under local measurements we mean measurements at AMON locations and at relevant places where atomic oxygen is created before it is transported to place where airglow is produced and observed by AMON instrument.

The declared aim is wide and include research of:

(a) geomagnetic field model precision during disturbed periods,

(b) models of upper atmosphere response to changes of global geomagnetic indexes.

In this chapter we focus on the first part (a). Geomagnetic field is a sum of field from internal Earth sources and external fields from current systems in the magnetosphere. We selected geomagnetic field models International Geomagnetic Reference Field (IGRF) [31] and Tsyganenko 05 [32] [33] as most relevant options available today. IGRF is model of internal sources of geomagnetic field and Tsyganenko 05 is model of external sources. IGRF is model of magnetic field created inside of Earth. Field from internal sources change very slowly in comparison with time scale of geomagnetic storms. Geomagnetic field from internal sources

change less than $\sim 0.1\,\mathrm{nT}$ per day at Earth surface, while geomagnetic storm create changes with order of $100\,\mathrm{nT}$ per day. Major part of geomagnetic field dynamics during storms is caused by external geomagnetic field.

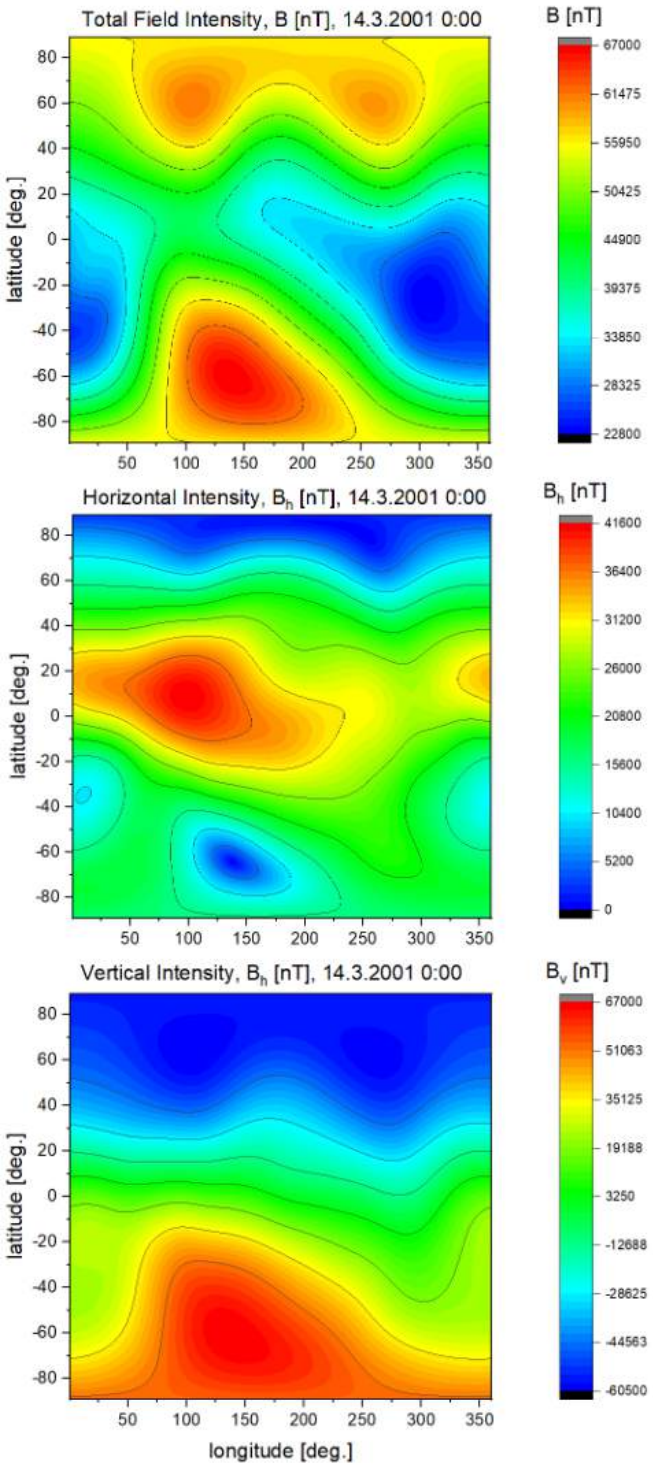

Figure 5.1: *Top:* The global map of total geomagnetic field intensity. *Middle:* Horizontal component of geomagnetic field intensity. *Bottom* Vertical component of geomagnetic field intensity. All panels are for the same date 14 March 2001.

At first, we evaluated dynamics of geomagnetic field in previous two solar periods, to have all types of geomagnetic activity from very quiet periods to very disturbed periods. We evaluated global geomagnetic field for 64,800 points at Earth surface (net of 360 x 180 positions with 1 degree step in latitude and longitude). The mentioned 64,800 positions represent a global map. We evaluated global maps with one hour time step, i.e. 24 x 365 = 8760 maps per one year. The example of global map of total intensity of geomagnetic field at Earth surface for 14 March 2001 at 00:00 UT is presented in Figure 5.1. In that moment magnetosphere was quiet with Dst index equal -16 nT.

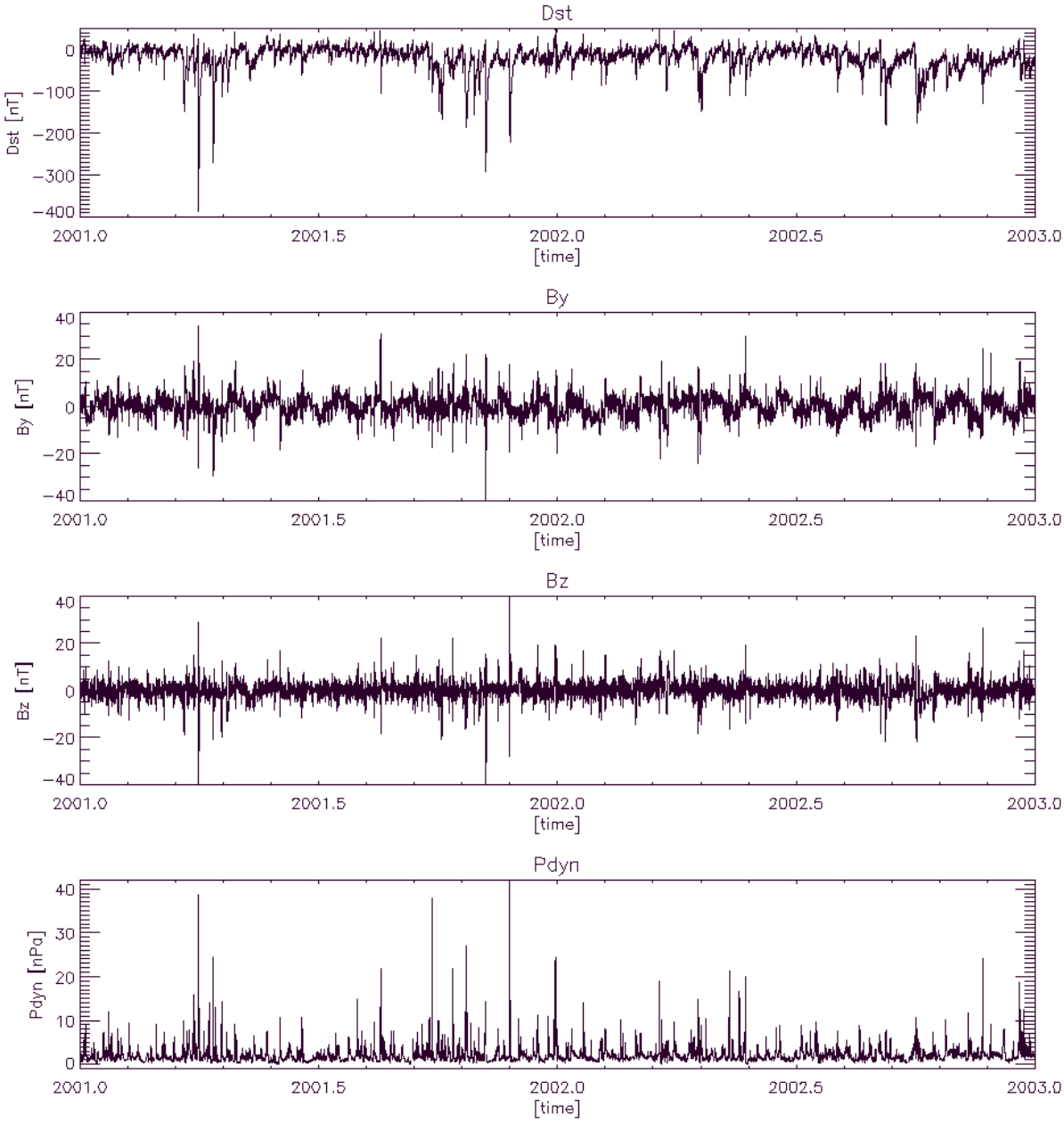

Figure 5.2: The parameters Dst (global geomagnetic field index), By, Bz (components of interplanetary magnetic field at 1 AU), and pdyn (dynamic pressure of solar wind) in years 2001 and 2002 with 1 hour time step.

The Tsyganenko 05 geomagnetic field model use following input parameters describing situation in interplanetary space and magnetosphere: By, Bz, pdyn, Dst and W1, W2, W3, W4, W5, W6. The parameters By and Bz are components of interplanetary magnetic field at 1 AU (coordinate system where x axis is directed toward the Sun, x and y axis are parallel to ecliptic and z axis is perpendicular to ecliptic), pdyn is dynamic pressure of solar wind, Dst is global geomagnetic field index and W1–W6 are parameters describing a prehistory of magnetosphere geomagnetic field. The example of By, Bz, pdyn, Dst evolution in years 2001 and 2002 is in Figure 5.2. As one can notice, there were couple of strong geomagnetic storms in year 2001. First and most strong one was on 31 March 2001 when at 00:00 was Dst=0 nT and 8 hours later storm reached Dts=-387 nT. Kp index changed from 3+ before storm to level 9- during two consecutive 3-hours periods from 03:00 to 08:00 UT.

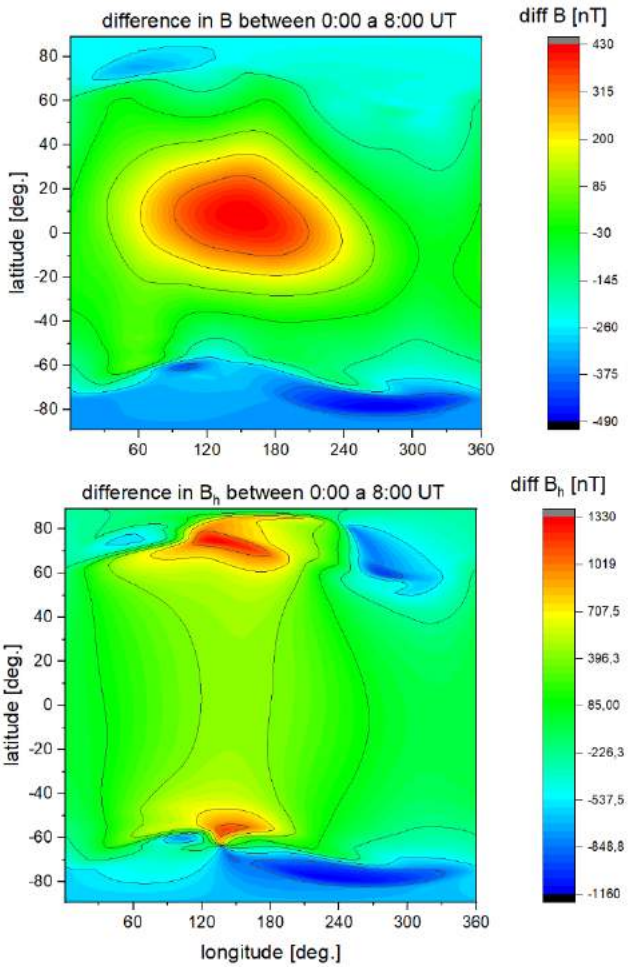

Figure 5.3: The difference before and after the geomagnetic storm in total geomagnetic field intensity *(upper panel)* and in horizontal geomagnetic field *(bottom panel)*.

To show example how geomagnetic field was changed globally during those storms, we prepared Figure 5.3. It presents the comparison of geomagnetic field before storm (00:00 UT) and in the moment when storm reached the maximum of its intensity (08:00 UT). The upper panel in Figure 5.3 displays the change of total field intensity between 00:00 UT and 08:00 UT of 31 March 2001. The bottom panel displays difference in horizontal component of

geomagnetic field. As it could be noticed, the total field was changed in smaller range than the horizontal component. Bottom panel nicely illustrates why different stations of Kp network has different maxima for Kp index equal to 9. Generally, stations with higher geomagnetic latitudes experience higher disturbances in horizontal component of geomagnetic field.

The field components evaluated from geomagnetic model and Dst index are presented for Lerwick (Scotland, 60°08' N 358°49') and Fredericksburg (USA, 38°12' N 282°38') stations of Kp network in Figure 5.4. Note that horizontal component in Lewerick evaluated by model was changed during the storm almost $\sim$ 1200 nT. Local limit for Kp=9 for Lerwick is 1000 nT. In Fredericksburg horizontal field component was changed $\sim$ 350 nT, what is under the local limit 500 nT for Kp=9 at this station.

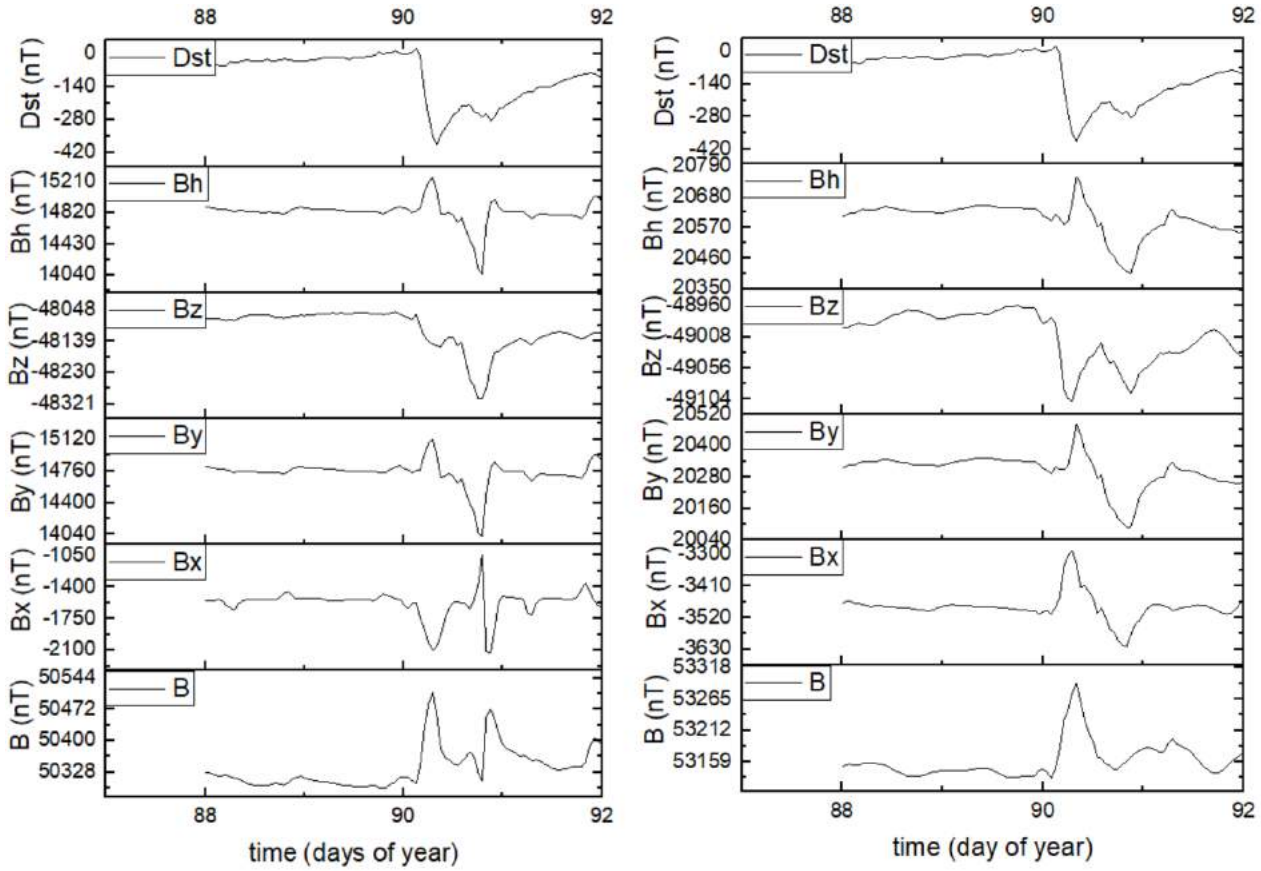

Figure 5.4: The Dst index and calculated geomagnetic field components for Lerwick (*(left panel)*) and Fredericksburg *(right panel)* station during geomagnetic storm on 31 March 2001.

To show example of time evolution of geomagnetic field intensity at AMON-net locations, we take positions of AMON-net observatories from the evaluated maps and present mentioned geomagnetic storms in locations ORM - Mexico, OAN - La Palma (Spain) and in AOK - Kolonica (Slovakia). The calculated horizontal intensity of geomagnetic field in Mexico during storm on 31 March 2001 changed $\sim$ 200 nT (see Figure 5.5). In La Palma it was 380 nT and in Kolonica 430 nT.

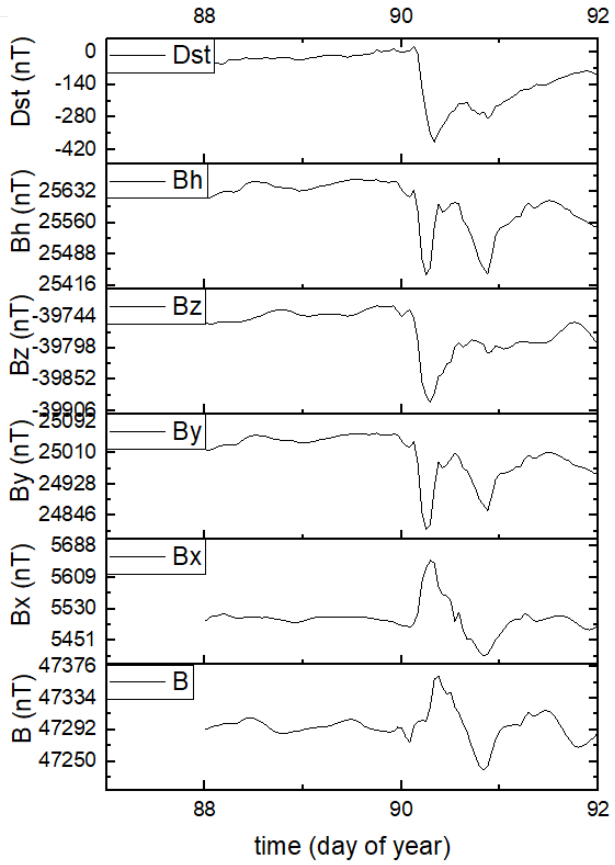

Figure 5.5: The Dst index and calculated geomagnetic field components for AMON location in Mexico during geomagnetic storm on 31 March 2001.

The created archive of global maps contain data of local geomagnetic field dynamics during disturbed periods at AMON-net locations during previous two solar cycles. The next steps will include

- comparison of geomagnetic field model results with measurements at Kp observatories positions from intermagnet.org database
- evaluation of local K indexes from measurements at intermagnet.org and evaluation of local K indexes from model results
- finding out closest measurements of geomagnetic field to AMON-net positions, evaluate K indexes from those measurements and comparison with K indexes evaluated from model at AMON-net positions.

Comparison of local K indexes with planetary Kp indexes were done for Fredericksburg observatory in article [34]. Authors concluded that local indexes may be recorded with smaller local K values at the North America. This is in agreement with geomagnetic field model results calculated for geomagnetic storm on 31 March 2001.

Chapter 6

Conclusions and Next steps

The objective of this Technical Note of Theoretical Study (TN-TS) was to provide theoretical background that is needed for other activities within SK2-09. Basically, it contains a continuation of preparatory activities that were performed within SK1-05. We have presented the basic characteristics of the Earth's upper atmosphere and the connection between the neutral part - thermosphere and the ionized part - ionosphere. Then we have described main airglow emissions and their usefulness for monitoring of upper atmosphere in different altitudes. The main phenomena that play the role in thermosphere-ionosphere dynamics have been specified and their studies by airglow observations have been explored. The conclusion from this part is that the monitoring of airglow is a valuable tool for detection of upper atmosphere dynamics. It is useful for characterization of variations that take years as well as for detection of variations with duration of several minutes.

The upper atmosphere is very complicated system and the monitored parameters are usually consequence of several phenomena that act in the same time. To distinguish between these sources, high number of data are needed to provide sufficient statistics. For this purpose, we have employed historical airglow data measured by photometers that could be used as an additional source of information to the AMON-net data. The first results from historical airglow data prove their usefulness as they are consistent with the generally published results.

As it is presented throughout whole TN-TS, the upper atmospheric dynamics and the various disturbances occurred locally. They are not uniform in time and for different locations. Therefore the correlation with the global indexes (e.g. Kp, Dst, etc.) might be not so straightforward. To take into account local effects of geomagnetic field dynamics, we have employed the models of internal (IGRF) and external (Tsyganenko 05) geomagnetic field. This might be a very useful approach for characterization of evaluation of local geomagnetic field dynamics during disturbed periods at particular AMON-net locations.

The next steps in theoretical study will consists of direct connection between theoretical knowledge published by other authors with the measurements provided by AMON-ES and AMON-net. This synthesis will lead to operation of reliable network of airglow monitoring instruments that will provide valuable information about current state of the upper atmosphere.